

25.8 Gb/s Submillimeter Optical Data Link Module for Smart Catheters

Li, Jian; Li, Chenhui; Henneken, Vincent; Louwerson, Marcus; Van Rens, Jeannet; Dijkstra, Paul; Raz, Oded; Dekker, Ronald

DOI

[10.1109/JLT.2021.3137981](https://doi.org/10.1109/JLT.2021.3137981)

Publication date

2022

Document Version

Final published version

Published in

Journal of Lightwave Technology

Citation (APA)

Li, J., Li, C., Henneken, V., Louwerson, M., Van Rens, J., Dijkstra, P., Raz, O., & Dekker, R. (2022). 25.8 Gb/s Submillimeter Optical Data Link Module for Smart Catheters. *Journal of Lightwave Technology*, 40(8), 2456-2464. <https://doi.org/10.1109/JLT.2021.3137981>

Important note

To cite this publication, please use the final published version (if applicable). Please check the document version above.


Copyright

Other than for strictly personal use, it is not permitted to download, forward or distribute the text or part of it, without the consent of the author(s) and/or copyright holder(s), unless the work is under an open content license such as Creative Commons.

Takedown policy

Please contact us and provide details if you believe this document breaches copyrights. We will remove access to the work immediately and investigate your claim.

25.8 Gb/s Submillimeter Optical Data Link Module for Smart Catheters

Jian Li , Chenhui Li , Vincent Henneken, Marcus Louwerse, Jeannet van Rens, Paul Dijkstra, Oded Raz , *Member, IEEE*, and Ronald Dekker

Abstract—The digitization of smart catheters will dramatically increase the demand for reliable and high data transmission in the distal tips. Optical fiber is a good candidate to provide high-speed data transmission. However, the extremely small size of the smart catheter tip, with less than a few millimeters in diameter, hampers the integration of optical fiber connections in the catheter tip. Our work presents a stand-alone optical data link module (ODLM) with a dimension of $240\ \mu\text{m} \times 280\ \mu\text{m} \times 420\ \mu\text{m}$ for use in a 1 mm diameter intravascular ultrasound (IVUS) smart catheter. The fabrication of the ODLM is based on the Flex-to-Rigid (F2R) integration technology. In the ODLM, the flexible interconnects reroute the electrical contacts of the flip-chipped vertical-cavity surface-emitting laser (VCSEL) to the side of the device. This design enables the ODLM to be mounted on a flex-PCB and fit into a 200–300 μm gap in the IVUS catheter tip. An optical fiber that runs parallel to the catheter shaft is self-aligned to a commercially available VCSEL by inserting it into the through-silicon hole (TSH) of the ODLM. Clear eye diagrams prove the stand-alone ODLM can transmit 25.8 Gb/s, $2^{31}-1$ Pseudo-Random Binary Sequence (PRBS) when driven through a high-speed bias-tee. The BER test indicates that error-free operation can be achieved at an optical output of around $-4\ \text{dBm}$.

Index Terms—Flex-to-rigid, microassembly, microfabrication, optical interconnections, optical transmitters, smart catheters.

I. INTRODUCTION

IN 2016, cardiovascular diseases (CVDs) accounted for around 17.9 million deaths, representing 31% of global deaths [1]. Now, smart catheters with a diameter of only a few

millimeters are being developed that function as the “eyes and ears” of the cardiologists to diagnose and treat most CVDs. Compared to conventional catheters, smart catheters have one or multiple sensors integrated into the distal catheter tip. Therefore, smart catheters need to send and receive information between the proximal and distal ends to transport the sensors data (e.g., temperature and pressures [2]–[6]). In this paper, we chose to work with intravascular ultrasound (IVUS) imaging catheter with a diameter of only 1 mm, as an example of a smart catheter. The application of IVUS catheters is in angioplasty surgery, also known as “stenting.” It is a minimally invasive procedure that restores the blood flow of a diseased coronary artery. First, a 360 μm diameter guidewire is inserted to the position of the diseased coronary artery to guide the other instruments. Next, an IVUS catheter can be slid over the guidewire, reaching the point of intervention to diagnose the diseased coronary artery and hence select the optimal dimension and position for stenting (Fig. 1(a)) [7]. The distal tip of the IVUS catheter contains an ultrasound transducer array for imaging and application-specific integrated circuits (ASICs) for signal processing. The imaging signals generated by the smart tip are transmitted to the proximal side of the catheter to build 2D or 3D cross-section images or videos of the diseased coronary artery.

Current IVUS catheters are all analog devices, which has several disadvantages. The analog transmission cables are very sensitive to the operating environment. The assembly costs to integrate the analog cables in a tiny catheter tip are up to 80% of the total catheter cost. In order to improve the signal integrity and reduce the assembly costs, the next generation of IVUS catheters will require digitization at the distal tip. As a result of data channel serialization, it is estimated that a data rate of 1.6 Gb/s is required based on the number of transducers, sample rate, and dynamic range. Compared to conventional copper micro coaxial cables, fiber optics has the inherent advantage of providing a data rate of more than 10 Gb/s per fiber [8]. However, unlike copper micro coaxial cables that can be directly connected to a PCB, the optical fiber must be accurately aligned and connected to a light source via an optical link. In our work, we designed and fabricated such an optical data link module (ODLM) for the IVUS catheter. The ODLM can also be used in other smart catheters for optical data communications.

Several optical interconnections and coupling schemes have been proposed in previous studies. However, they are mostly in a few millimeter scales [9]–[11]. In 2012, Fandrey *et al.* reported on a small optical link that fits in a catheter with a

Manuscript received September 6, 2021; revised November 23, 2021; accepted December 19, 2021. Date of publication December 23, 2021; date of current version April 18, 2022. This work was supported by the European project POSITION-II under Grant Ecsel-783132-Position-II-2017-IA.

Jian Li is with the Electronic Components, Technology and Materials (ECTM) group, Delft University of Technology, 2628 CD Delft, The Netherlands (e-mail: j.li-10@tudelft.nl).

Chenhui Li and Oded Raz are with the Department of Electrical Engineering, Eindhoven University of Technology, 5600 MB Eindhoven, The Netherlands (e-mail: chenhui.li@tue.nl; o.raz@tue.nl).

Vincent Henneken and Jeannet van Rens are with the Philips Research, 5656 AE Eindhoven, The Netherlands (e-mail: vincent.henneken@philips.com; jeannet.van.rens@philips.com).

Marcus Louwerse and Paul Dijkstra are with the MEMS and Micro Devices (MMD), Philips, 5656 AE Eindhoven, The Netherlands (e-mail: marcus.louwerse@philips.com; paul.dijkstra@philips.com).

Ronald Dekker is with the Electronic Components, Technology and Materials (ECTM) group, Delft University of Technology, 2628 CD Delft, The Netherlands, and also with the Philips Research, 5656 AE Eindhoven, The Netherlands (e-mail: r.dekker@tudelft.nl).

Color versions of one or more figures in this article are available at <https://doi.org/10.1109/JLT.2021.3137981>.

Digital Object Identifier 10.1109/JLT.2021.3137981

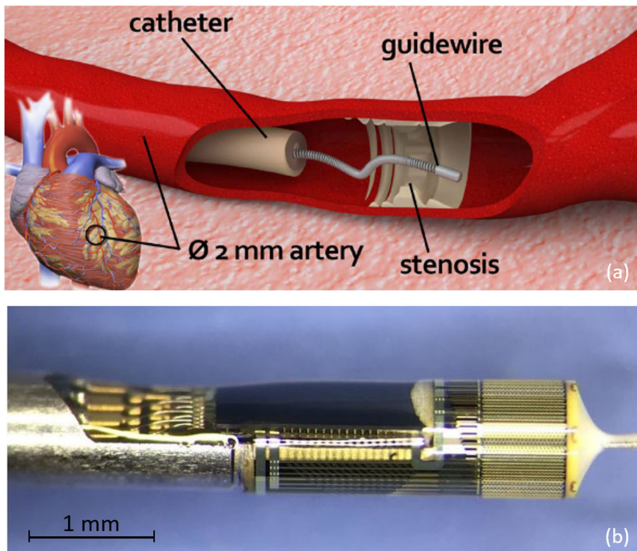


Fig. 1. (a) IVUS catheter sliding over the guidewire, reaching the intervention point, and acquiring ultrasound images. (b) Smart tip of the IVUS catheter developed by Philips Research.

diameter of 2.33 mm [12]. Nevertheless, the extremely small scale of the IVUS catheter requires further miniaturization of the optical link. As shown in Fig. 1(b), the distal tip of the IVUS catheter has a cylindrical outer wall with a diameter of 1 mm and a rigid length of approximately 8 mm. There is a guidewire lumen at the center of this cylindrical shape with a diameter of 500 μm . With this lumen, the IVUS catheter runs over the guidewire and is led to the location of the intervention. The only available space for an optical link in the IVUS catheter is the narrow gap of around 200–300 μm in between the outer wall of the catheter and the guidewire lumen. In addition, integrating an optical link into such an IVUS catheter raises assembly challenges. The IVUS catheter smart tip is a complex micro-electro-mechanical system consisting of multifunctional integrated stand-alone components. These components are all manufactured separately and assembled onto a thin flex-PCB in the final integration step. A 40 μm -thick flexible PCB with all the components is wrapped around the central lumen, making the most optimal use of the limited available space at the catheter tip. The optical link should be massively producible and must be a stand-alone device to align with the overall standard catheter assembly protocol.

In the next sections of this paper, we present the design concept and the device fabrication, which is part of our previous work [13]. We extend our previous work with the ODLM device assembly and evaluation in the final sections of this paper.

II. DESIGN CONCEPT

To solve the integration and miniaturization challenges, the ODLM was designed and fabricated in the well-established Flex-to-Rigid miniaturization technology. This section first gives a brief introduction to the F2R integration technology. Next, the F2R based design concept for the ODLM is discussed.

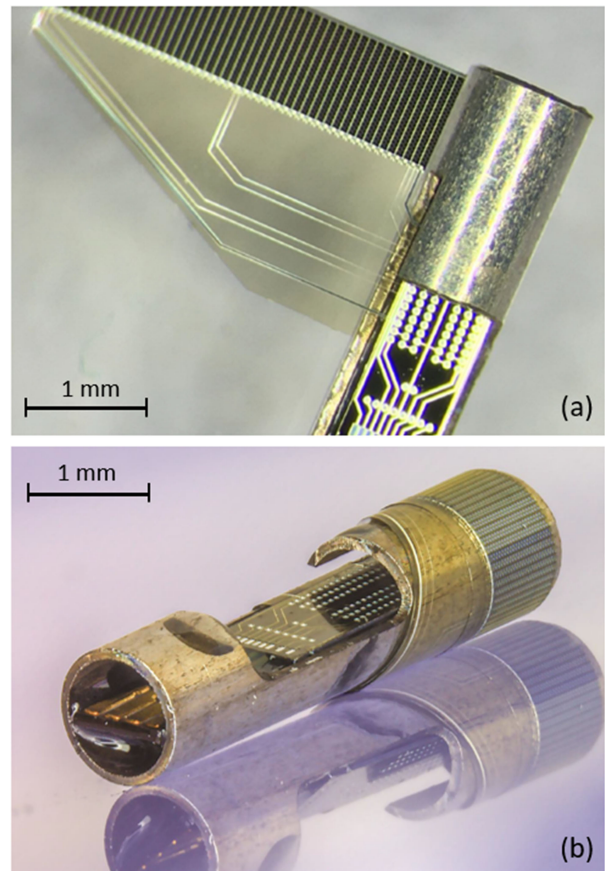


Fig. 2. An IVUS catheter tip based on the F2R technology developed by Philips Research in the ENIAC “INCITE” European project (grant no. 621278-2). (a) The ultrasound transducers are fabricated on the F2R silicon slits connected by flexible interconnects; (b) The ultrasound transducers on F2R silicon slits are wrapped around the 1.2 mm diameter stainless steel tube as the smart catheter tip.

A. Flex-to-Rigid (F2R) Integration Technology

F2R is a novel IC-compatible micro-fabrication technology for miniaturized system integration. It contains multiple isolated thin silicon islands that are connected by polymer-metal-polymer structured flexible interconnects. Devices can be directly fabricated or assembled onto the silicon islands. Due to the flexible connections, the silicon islands in the F2R system can be folded into arbitrary shapes to facilitate extremely small form-factor integration [14], [15]. Fig. 2 shows the application of the F2R technology in the production of an IVUS catheter tip. In Fig. 2(a), ultrasound transducers are fabricated on each rigid silicon slit connected by flexible interconnects. These semi-flexible structures are then wrapped around the catheter tip with a diameter of only 1.2 mm (Fig. 2(b)).

B. Design of Optical Data Link Module (ODLM)

The optical data link module comprises three parts. The first part is a micro-fabricated F2R silicon interposer. The second part is a commercially available Vertical Cavity Surface Emitting Laser (VCSEL), with its electrical contacts and laser emitting spot on the same surface. The final part is a 125 μm diameter optical fiber. The F2R silicon interposer incorporates flexible

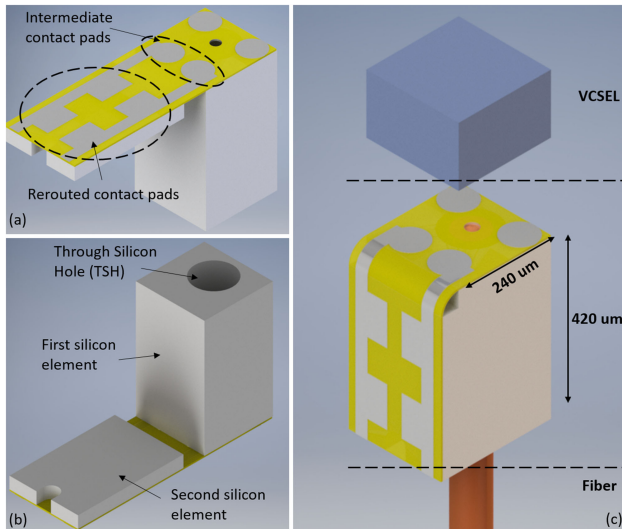


Fig. 3. ODLM design. (a) Unassembled F2R interposer; (b) backside view of unassembled F2R interposer; (c) assembled F2R interposer with flip chipped VCSEL and inserted optical fiber.

interconnects to reroute the VCSEL electrical contacts to a plane perpendicular to the surface of the VCSEL. This design enables the optical link module to be mounted on a flex-PCB within the limited space available in the catheter. At the same time, the VCSEL is optically aligned and connected to a fiber running in parallel to the catheter shaft.

Fig. 3 presents different views of the ODLM. The F2R interposer in Fig. 3(a)–(b) consists of two silicon elements connected by 6 μm -thick flexible interconnects. The first silicon element is a cuboid-shaped element with a planar dimension of $240\ \mu\text{m} \times 240\ \mu\text{m}$ and a thickness of $420\ \mu\text{m}$. The intermediate contact pads for the VCSEL connection are fabricated on the $240\ \mu\text{m} \times 240\ \mu\text{m}$ top surface. A through-silicon hole (TSH) located at the emitting area of the VCSEL connects the backside to the front side of the structure. The VCSEL (ULM850-14-CHIPS), with dimensions of $240\ \mu\text{m} \times 240\ \mu\text{m}$, and a thickness of $150\ \mu\text{m}$, is flip-chipped onto the intermediate contact pads with its laser emitting spot aligned to the TSH. Both the TSH and the intermediate contact pads are designed according to the VCSEL layout. Therefore, a multimode optical fiber inserted into the TSH from the bottom side will be self-aligned to the laser emitting spot of the VCSEL on the other side (Fig. 3(c)). The flip-chip assembly techniques guarantee an alignment accuracy within $5\ \mu\text{m}$ [16], sufficiently accurate to align a standard multimode fiber. The TSH also serves as mechanical support for the multimode optical fiber. With a small amount of (epoxy) adhesive, the fiber can be fixated in the optical TSH, and a reliable connection can be guaranteed.

The second silicon element has planar dimensions of $240\ \mu\text{m} \times 380\ \mu\text{m}$ and a thickness of $40\ \mu\text{m}$. The rerouted contacts for the PCB connection are fabricated on top of the $240\ \mu\text{m} \times 380\ \mu\text{m}$ surface. Flexible interconnects connect the rerouted electrical contacts to the intermediate contact pads on which the VCSEL is mounted. Initially, after the fabrication, the rerouted contact pad surface of the thin silicon element is in the same plane as the intermediate contact pad surface

of the cuboid silicon element. The flexible interconnect allows the folding of the thin silicon element by 90 degrees onto the side of the cuboid silicon element, where it is attached with an adhesive, as shown in Fig. 3(c). Hence, the folding separates the VCSEL laser emitting spot and the rerouted electrical contacts into perpendicular planes. After the assembly, the final size of the entire ODLM is $240\ \mu\text{m} \times 280\ \mu\text{m}$ with a height of $420\ \mu\text{m}$. The dimensions are adjustable based on the choice of the VCSEL. By connecting the rerouted electrical contacts to a flex-PCB, the optical link module acts as a stand-alone device that can be positioned inside the $200\text{--}300\ \mu\text{m}$ gap inside the IVUS catheter and other components shown in Fig. 4.

III. FABRICATION

The schematic representation of the ODLM F2R interposer fabrication flow is given in Fig. 5. The starting point for the processing is SOI wafers with a device layer thickness of $40\ \mu\text{m}$ and a handle layer thickness of $380\ \mu\text{m}$. The first step is to deposit and pattern a two-step etching mask onto the backside of the wafer for the deep reactive ion etching (DRIE) process (Fig. 5(a)). Next, the key feature of F2R, “buried trenches”, is fabricated into the SOI device layer. In the buried trench process, a thin plasma-enhanced chemical vapor deposition (PECVD) oxide layer is first deposited and patterned into a mesh mask for the buried trench etching process (Fig. 5(b)–(c)). The buried trenches are etched by DRIE using the oxide mesh mask. During DRIE etching through the oxide mesh mask, the under-etch of the DRIE process merges the mesh patterns and eventually forms a larger trench. Finally, the oxide mesh mask is closed by a thick PECVD oxide layer, resulting in closed buried trenches [17]. An example of the open/closed buried trench SEM image is shown in Fig. 5(d).

After the closure of the buried trenches, the surface of the wafer is intact again, which allows the first polyimide layer to be coated and cured. Contact vias are etched into the polyimide, landing on the oxide layer to provide the contact pads on a rigid substrate. AlCu is sputtered on the first polyimide layer and patterned into the routing interconnects. Subsequently, the second polyimide layer is coated and cured. Before backside processing, a metal hard etch mask layer is deposited and patterned on the second polyimide layer for the final polyimide etching step after backside processing has been completed, Fig. 5(e)–(f).

Fig. 5(g)–(i) presents the backside processing. The TSH in the ODLM design has a diameter of around $135\ \mu\text{m}$. In contrast, the entire silicon substrate underneath the second silicon element needs to be removed to release the thin silicon island. Because of the higher aspect ratio of the TSH compared to the larger open area, a two-step backside etching method is applied to guarantee a reliable TSH opening process. The oxide mask is patterned into two levels: the first level is the TSH pattern that lands on silicon, the second level is the larger open area pattern that is half etched into the oxide mask. The first backside silicon DRIE pre-etches the TSH $120\ \mu\text{m}$ into the silicon substrate (Fig. 5(g)). Next, the oxide mask is thinned down to expose the larger open area mask (Fig. 5(h)). Now the larger area and the TSH are etched together to land on the SOI buried oxide. The SOI buried oxide and the oxide layer underneath the flexible interconnects are

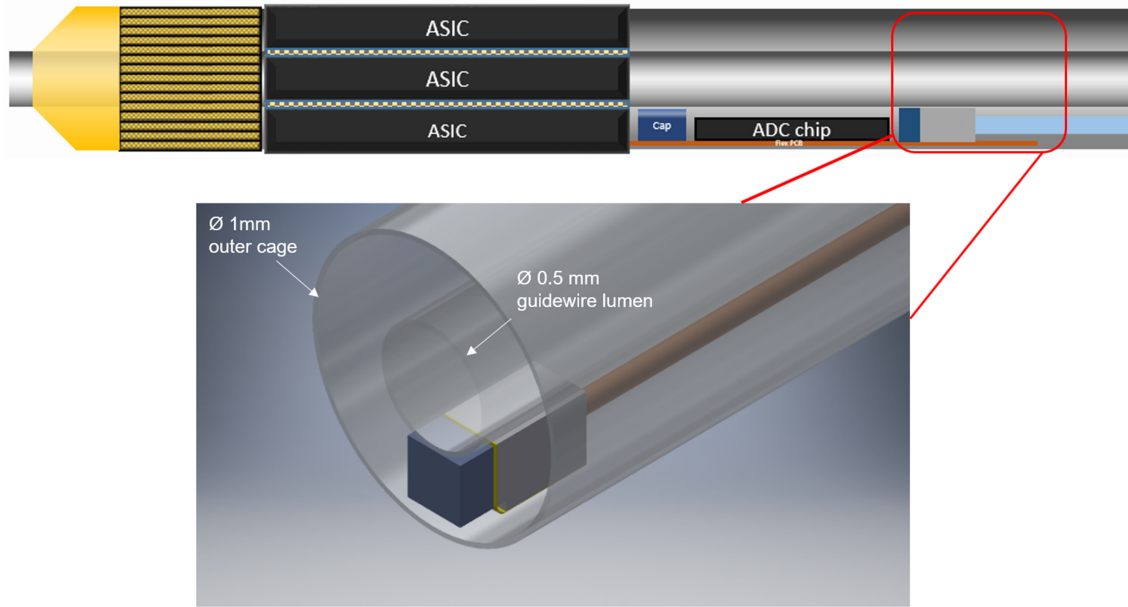


Fig. 4. Integration layout of an ODLM connected to a flex-PCB in the 200–300 μm gap inside the IVUS catheter tip between the inner guidewire lumen and the outer wall.

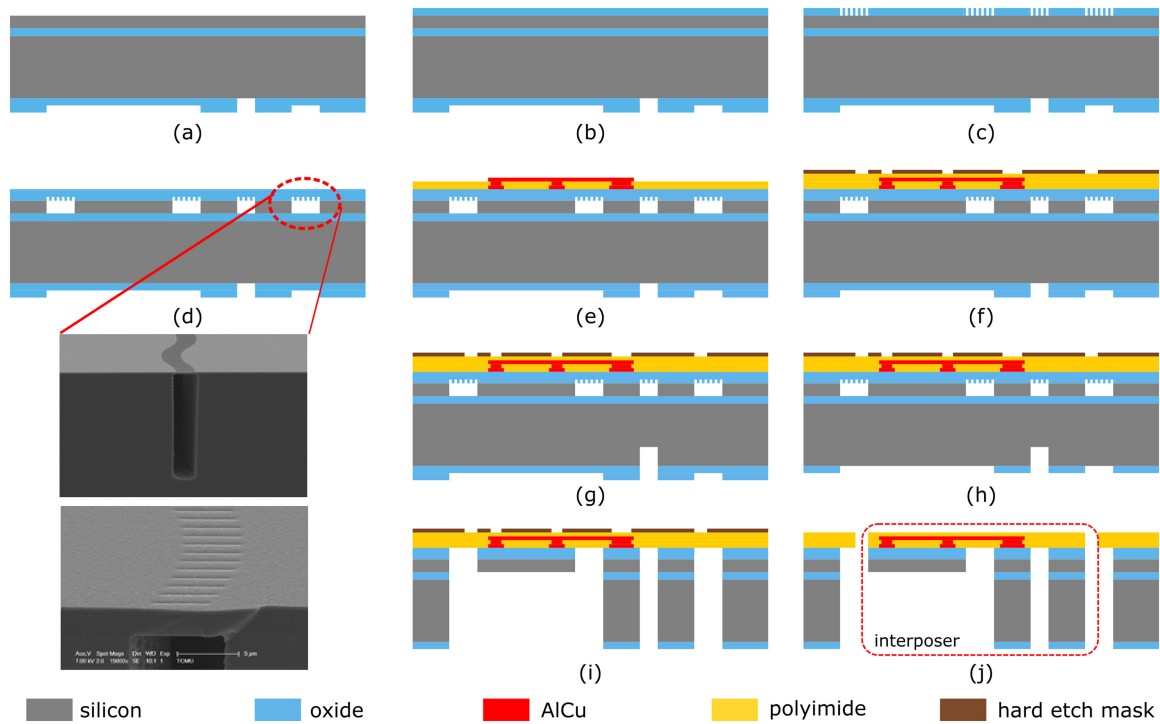


Fig. 5. Schematic representation of the ODLM F2R interposer fabrication flow. (a) Two-step backside etching mask processing. (b,c) Deposition and patterning of PECVD oxide for buried trench etching. (d) Etching of the buried trench with DRIE and closing with a thick PECVD oxide layer. SEM cross-section of the opened/closed buried trench is shown. (e) Coating the first polyimide layer, etching of vias to the oxide layer, and processing of AlCu interconnects. (f) Deposition of the second polyimide layer and hard etch mask for contact pad opening. (g) The first backside etch. (h) Thinning down of the two-step backside etching mask. (i) The second backside etch. (j) Etching of the polyimide to open contact pads and release the F2R structures.

subsequently removed from the backside with a high-pressure oxide dry etch (Fig. 5(i)). Finally, using the prefabricated hard etch mask on the front side of the wafer, a front side polyimide etch opens the contact pads and releases the device. A wet etch process removes the hard etch mask (Fig 5(j)). Because of the PI-metal-PI sandwiched structure, the metal layer in the

flexible interconnect is in the stress-neutral plane. Therefore, the flexible interconnect can achieve a very small bending radius of 10 μm [18].

Fig. 6 presents some details of the fabricated ODLM F2R interposer. Fig. 6(a) shows the front side view of the F2R interposer attached to the silicon frame by polyimide tabs. The silicon

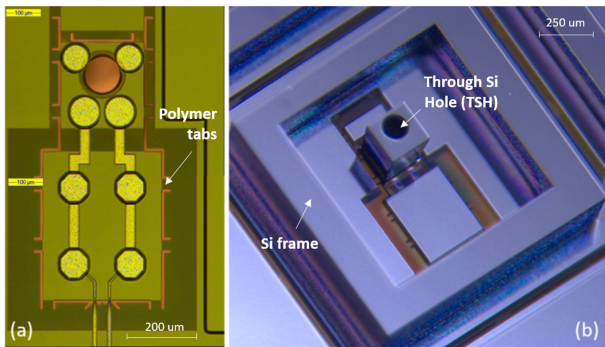


Fig. 6. ODLM F2R interposer fabrication results. (a) Front side view of the F2R interposer attached to the silicon frame. (b) Backside view of the F2R interposer in the silicon frame.

frame alleviates the handling difficulties during the device assembly. A basic electrical open & short measurement confirms the successful opening of the contact pads and the functionality of the flexible interconnects. By applying backside illumination, clear light can be observed from the front side through the TSH, which indicates the correct opening of the TSH. Fig. 6(b) shows the backside view of the ODLM F2R interposer attached to the silicon frame. The backside DRIE process only results in 10 μm under-etch after etching the 380 μm thick silicon handle layer. The backside DRIE process defines the first and second silicon elements and releases them from the Si substrate.

IV. ASSEMBLY AND PACKAGING

After fabrication, the ODLM F2R interposer is attached to the Si frames by polymer tabs and remains in the Si wafer. To assemble the VCSEL to the intermediate contact pads and form a reliable electrical connection for high-speed data transmission, we chose to flip-chip the VCSEL to the F2R interposer with solder spheres. The second Si island was then bent 90 degrees and glued to the side of the island holding the VCSEL. The main assembly challenge is to handle the extremely small VCSEL and the assembly surface. Moreover, all the ODLM structures are free-hanging in the Si frame during the assembly steps, which cannot provide a sturdy assembly surface. This section shows in detail how we dealt with the assembly challenges.

The contact pads were provided with an electroless Nickel electroless Palladium immersion gold (ENEPIG) under bump metallization by an external supplier (PacTech). The ENEPIG process resulted in a layer stack of around 3.2 μm of electroless Nickel, 400 nm electroless Palladium, and 60 nm Au. A solder wetting test proved that the contact pads had sufficient wettability to the solder spheres. With soldering flux (TSF6592 from Flux Kester), solder spheres (SAC305 from Mitsui) with a diameter of 60 μm were placed on the four contact pads. The soldering flux helps with the positioning of the tiny solder spheres and cleans the soldering surfaces. After a reflow bake of 30 seconds at 260 degrees in the ATV oven, the solder spheres were connected to the contact pads. The VCSEL was flip-chipped placed on top of the reflowed solder spheres. After a second reflow, the bottom two contact pads formed a good connection to the VCSEL. The solder spheres on the top two contact pads acted as mechanical

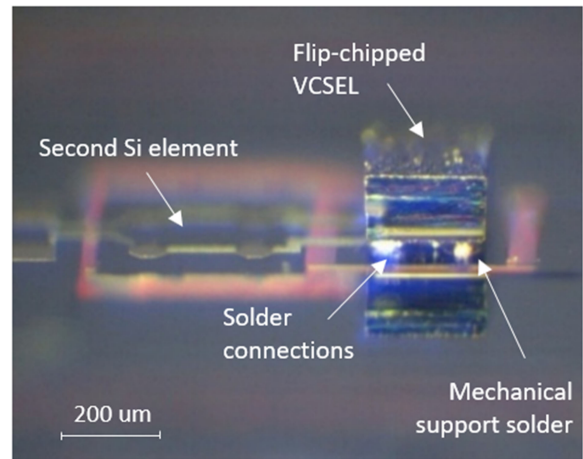


Fig. 7. VCSEL flip-chip assembly to the F2R interposer, the F2R interposer is still connected to a silicon frame by polymer tabs.

support to prevent VCSEL from tilting during the second reflow. Fig. 7 presents a side view of the complete ODLM with the VCSEL flip-chip assembled on the F2R interposer. The electrical connection was verified by probing the contact pads on the interposer and measuring the I-V curve of the VCSEL. The measured VCSEL IV curve showed a classic diode behavior with a threshold voltage of 1.4 V, indicating the successful VCSEL assembly.

The F2R interposer with the assembled VCSEL was released from the Si frame after the VCSEL placement (see Fig. 8(a)). The second thin silicon element was free hanging at this step and connected to the first silicon element by flexible interconnect. The second thin silicon element was folded by 90 degrees and fixated to the side of the first silicon element with a transparent biocompatible UV-cure glue (203A-CTH-F from DYMAX). We chose a 125 μm diameter pigtail OM1 multimode optical fiber with a large fiber core of 62.5 μm diameter to capture more optical output from the VCSEL. The jacket and the coating of the fiber were stripped at the tip of the pigtail side, leaving only the core and the cladding with a diameter of 125 μm . The stripped fiber tip was dipped in the same transparent bio-compatible glue, inserted into the 135 μm diameter through-silicon hole, and pushed to the assembled VCSEL on the other side. The fiber was eventually fixated by UV-curing. Fig. 8(b) depicts the final assembled stand-alone ODLM, including the VCSEL, the F2R inter-poser, and an inserted 125 μm diameter optical fiber.

V. RESULTS AND DISCUSSION

The ODLM was characterized by high-speed data transmission measurements. We first drove the stand-alone ODLM through a high-speed bias-tee, proving that the ODLM can transmit 25.8 Gb/s, $2^{31}-1$ PRBS. The eye diagrams and bit error rate (BER) test indicated that error-free operation can be achieved at an optical output of around -4 dBm. Next, the ODLM was assembled on a PCB with a customized laser driver ASIC optimized to deliver the best speed-power tradeoff for the IVUS application. The entire integrated system can transmit 7 Gb/s, $2^{15}-1$ PRBS. The characterization setups and integration details are presented in this section.

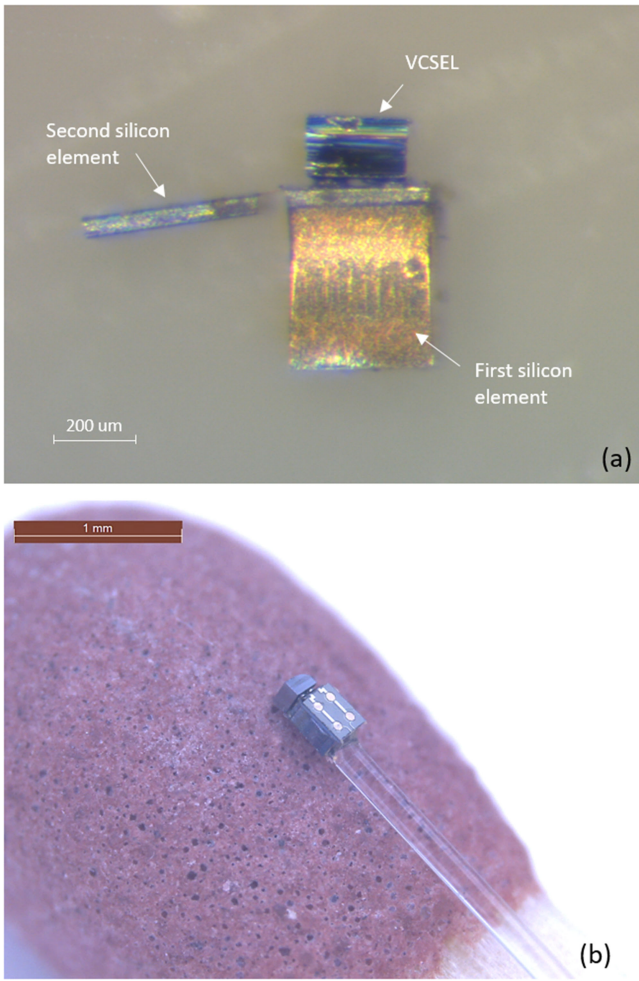


Fig. 8. (a) Side view of an ODLM F2R interposer with assembled VCSEL, released from the Si frame. The two silicon elements are connected by flexible interconnects. (b) An assembled ODLM, with the VCSEL and an inserted 125 μm diameter optical fiber, placed on a match head. Optical fiber was fixated by biocompatible glue.

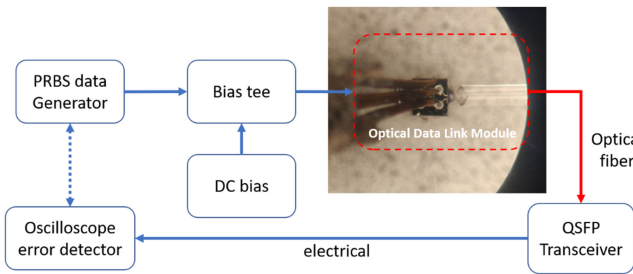


Fig. 9. Scheme of signal integrity testing setup for the stand-alone ODLM device, with an inserted microphotograph of the ODLM device being probed by high-speed differential probes.

A. Stand-alone ODLM

A scheme of the ODLM optical characterization setup is shown in Fig. 9. A DC bias voltage is applied to the VCSEL in the ODLM through a bias tee module to provide the bias voltage. The generated high-speed data is transmitted through the bias tee and fed into the ODLM using high-speed differential probes.

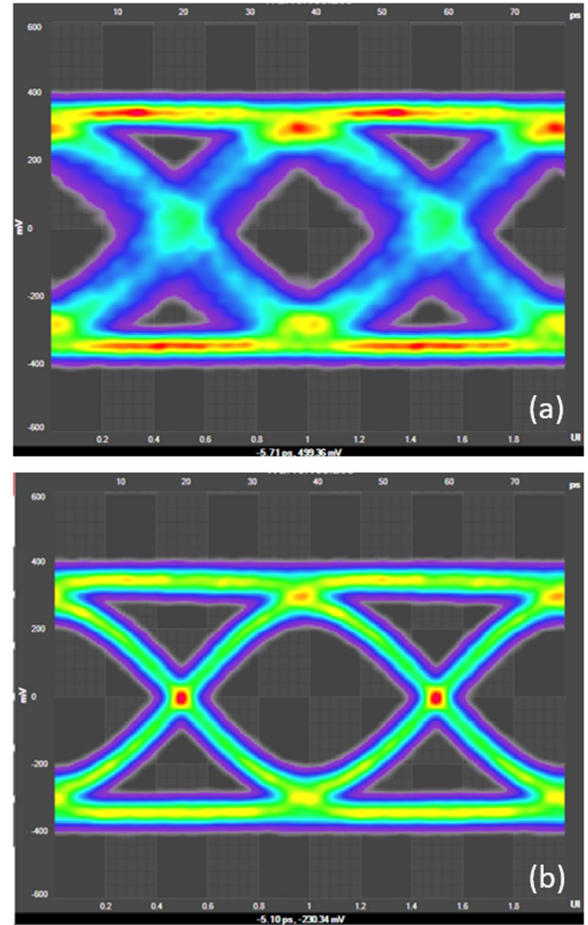


Fig. 10. Eye diagram of a stand-alone ODLM with 25.8Gb/s, PRBS $2^{31}-1$ sequence. (a) without CDR, (b) with CDR. (200 mV/div, 7.69 ps/div).

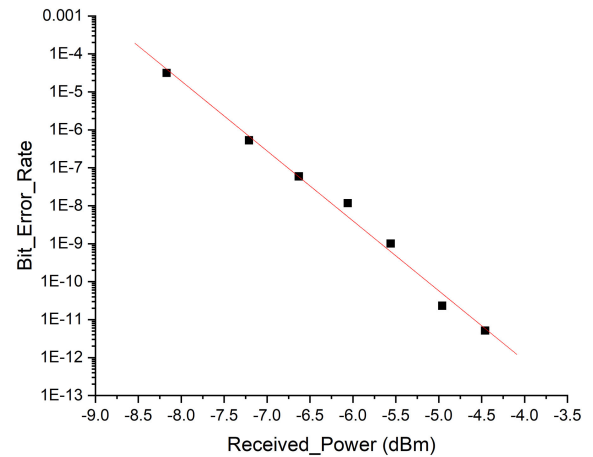


Fig. 11. Fitted BER curve for the stand-alone ODLM 25.8 Gb/s with PRBS 2^7-1 sequence transmitting test.

The data is converted to an optical signal, propagates through the optical fiber into a commercial QSFP (100G-SR4-S from Cisco) transceiver. The QSFP converts the optical signal to an electrical signal connected to an oscilloscope error detector. In this setup, the PRBS data generator and the oscilloscope error detector are

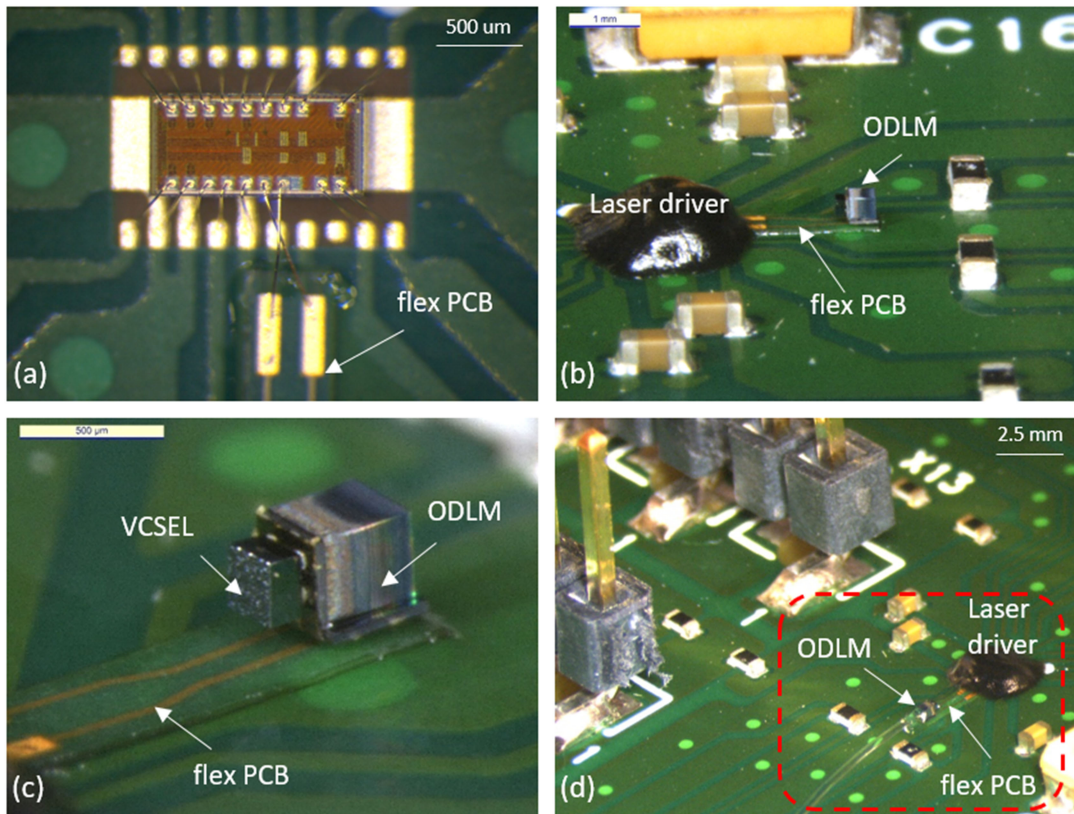


Fig. 12. ODLM connected to catheter laser driver with flex PCB. (a) Customized laser driver for catheter application, wire-bonded to the test PCB and the 40 μm -thick flex PCB; (b) ODLM is connected to laser driver via a flex PCB. The laser driver is in the black polymer glob top; (c) Side view of ODLM assembled on a flex PCB; (d) overall view of ODLM connected to the laser driver on a testing PCB.

integrated into one time-domain analyzer (ML4004-PAM from multiLane).

A bias voltage of 1.91 V was applied to obtain the best performance of the VCSEL. An optical output power $P_{\text{opt}} = 1.112$ mW was detected at the end of the 1 m long optical fiber. Compared with the specifications of the VCSEL, where $P_{\text{opt}} = 1.75$ mW is achieved at 1.91 V bias voltage, this stand-alone ODLM device delivered 63.5% of the optical intensity generated by the VCSEL. The received optical output power is dominated by VCSEL positioning and fiber coupling. The 25.8 Gb/s differential signal, with PRBS $2^{31}-1$ sequence, was fed into the ODLM device through high-speed probes. The converted electrical signal from the QSFP can be visualized on the oscilloscope in the analyzer. The eye diagrams, with and without clock data recovery (CDR), are shown in Fig. 10, proving the capability of the stand-alone ODLM to support data rates up to 25.8 Gb/s.

The bit error rate (BER) testing was performed with the same test setup. A 25.8 Gb/s differential signal with a PRBS 2^7-1 sequence was fed into the ODLM through the high-speed probes. The optical output was transmitted to the QSFP and converted to an electrical signal fed into the error detector. The BER testing result is shown in Fig. 11. The result shows how the BER varies as a function of the received optical power. It demonstrated that error-free ($\text{BER} < 10^{-12}$) data transmission can be achieved with an optical output of more than -4 dBm from the ODLM device. The BER at such a high data rate highly relies on the

entire communication system. The solder connections (such as contact resistance differences) between the VCSEL and ODLM, the interconnect traces on the ODLM, and the high-speed probe connection can contribute to bit errors.

B. ODLM Integrated With Catheter Laser Driver

The ODLM was originally developed as an optical link for a digital IVUS catheter to provide a data rate communication of ≥ 1.6 Gb/s. To demonstrate the functionality of the ODLM in an integrated digital IVUS system, a customized laser driver was designed and fabricated for a data rate of 6 Gb/s. Because the operating environment of the catheter is in the human body, the power dissipation of the laser driver must be less than 10 mW so that the temperature of the catheter does not exceed 40 degrees. Fig. 12 depicts the ODLM connected to the laser driver via a flex PCB. The laser driver was wire-bonded onto the PCB first, and then the ODLM was flip-chipped on a 40 μm -thick flex PCB. The flex PCB with the ODLM was subsequently fixated and wire-bonded to the laser driver. A black polymer glob top was applied to the assembled laser driver chip to protect the wire bonds. Finally, the optical fiber was inserted into the ODLM, and a transparent glob top was applied to the entire ODLM device.

Signal integrity tests were performed to evaluate the ODLM and laser driver assembly. A PRBS data generator (AWG7122B from Tektronix) transmits high-speed data to the laser driver. The

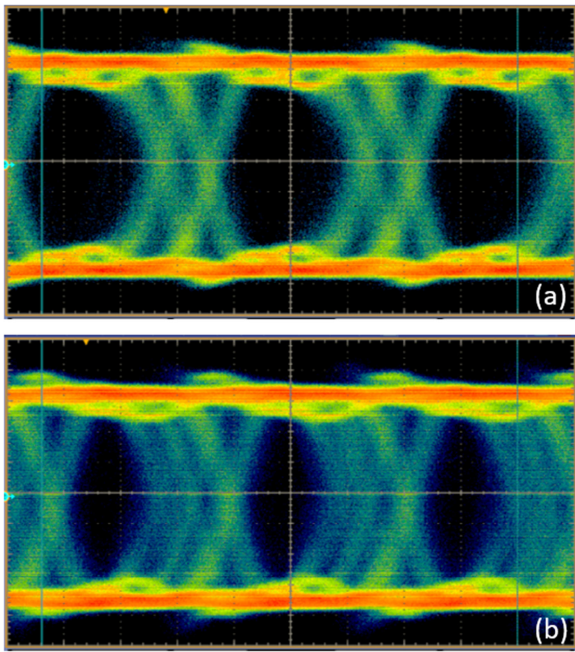


Fig. 13. Eye diagrams of ODLM & laser driver testing board with PRBS $2^{15}-1$ sequence (a) 7 Gb/s, (b) 8 Gb/s. (60 mv/div, 40 ps/div).

laser driver drives the ODLM and converts the electrical signal to an optical signal. The optical signal is fed into a QSFP transceiver and converted back to an electrical signal. A digital oscilloscope (DPO72004 from Tektronix) is used to visualize the eye diagram. A bias voltage of 1.94 V was applied to the ODLM device. An optical output power $P_{\text{opt}} = 1.065$ mW was detected at the end of the 1 m long optical fiber. Compared to the specifications of the VCSEL, where $P_{\text{opt}} = 1.43$ mW is specified at a bias voltage of 1.94 V, this assembled stand-alone ODLM device on the testing board delivered 74.5% of the optical intensity generated by the VCSEL. The difference in the received P_{opt} compared with the stand-alone version is most likely caused by the tilt of the VCSEL. 7 Gb/s and 8 GB/s differential signals, with $2^{15}-1$ sequence, were fed into the ODLM device through the laser driver. The converted electrical signals from the QSFP were visualized on the oscilloscope. The eye diagrams of the assembly are shown in Fig. 13. It seems that the customized laser driver over-performed and a clear eye diagram was achieved for a data rate of 7 Gb/s, as presented in Fig. 13(a). Due to the limitation of the measurement setup (e.g., signal trigger setting), eye pattern at 8 Gb/s suffers from large jitter and has smaller opening, as shown in Fig. 13(b). Nevertheless, a data rate of 7 Gb/s is more than sufficient for the digital IVUS catheter application, where a data rate of 1.6 Gb/s is required.

VI. CONCLUSION

An F2R based optical data link module (ODLM) with a dimension of $240 \mu\text{m} \times 280 \mu\text{m} \times 420 \mu\text{m}$ was designed, fabricated, assembled, and characterized. With a flip-chip assembled commercial VCSEL, the ODLM fits in the 200–300 μm gap between the inner lumen and outside wall in the IVUS

catheter tip. A 125 μm diameter optical fiber was connected by inserting it into the through silicon hole (TSH) of the ODLM and self-aligned to the emitting spot of the assembled VCSEL. Eye diagrams were used to characterize the optical performance of the ODLM. The stand-alone ODLM can transmit up to 25.8 Gb/s $2^{31}-1$ PRBS when driven through a high-speed bias tee. The BER test indicates that error-free operation can be achieved at an optical output of around -4 dBm. In addition, when integrated with a customized 6 Gb/s catheter laser driver, the ODLM can transmit 7 Gb/s $2^{15}-1$ PRBS.

The stand-alone submillimeter ODLM introduces optical data transmission for extremely small smart catheters, such as the IVUS catheter discussed in this paper. It is also possible to change the design of the ODLM based on different VCSELS so that it can be used in other applications. The ODLM can dramatically reduce the assembly costs and simplify the assembly process to integrate optical data transmission into a catheter system. In the future, the focus is to develop an industrial process. Some automated assembly steps can be introduced to improve the VCSEL flip-chip process. In addition, optimizing the impedance design in ODLM may further increase the data rate.

ACKNOWLEDGMENT

The authors would like to thank the extensive supports from the process engineers in the cleanroom of Micro System & Devices (MMD), Philips. We also appreciate the specialists, B. Jacobs, N. Rijkers, M. Broekman, R. van Rijswijk, and A. Sielecki from Philips Research, Philips Greenhouse, and Philips MMD, for their contributions to the device assembly and test.

REFERENCES

- [1] "Cardiovascular diseases (CVDs)," Accessed: Apr. 15, 2020. [Online]. Available: [https://www.who.int/news-room/fact-sheets/detail/cardiovascular-diseases-\(cvds\)](https://www.who.int/news-room/fact-sheets/detail/cardiovascular-diseases-(cvds))
- [2] T. Sharma, K. Aroom, S. Naik, B. Gill, and J. X. J. Zhang, "Flexible thin-film PVDF-TrFE based pressure sensor for smart catheter applications," *Ann. Biomed. Eng.*, vol. 41, no. 4, pp. 744–751, 2013.
- [3] C. Li *et al.*, "Smart catheter flow sensor for real-time continuous regional cerebral blood flow monitoring," *Appl. Phys. Lett.*, vol. 99, no. 23, 2011, Art. no. 233705.
- [4] C. Li *et al.*, "Brain temperature measurement: A study of in vitro accuracy and stability of smart catheter temperature sensors," *Biomed. Microdevices*, vol. 14, no. 1, pp. 109–118, 2012.
- [5] M. R. Brooks, S. F. Lee, D. L. Livingston, and J. C. Squire, "Smart catheter for stent placement," *IEEE Potentials*, vol. 22, no. 1, pp. 19–22, Feb./Mar. 2003.
- [6] X. Ji, P. Zhou, L. Zhong, A. Xu, A. C. O. Tsang, and P. K. L. Chan, "Smart surgical catheter for C-reactive protein sensing based on an imperceptible organic transistor," *Adv. Sci.*, vol. 5, no. 6, 2018, Art. no. 1701053.
- [7] R. Stoute, M. C. Louwerse, J. van Rens, V. A. Henneken, and R. Dekker, "Optical data link assembly for 360 μm diameter IVUS on guidewire imaging devices," in *Proc. IEEE Sensors*, 2014, pp. 217–220, doi: [10.1109/ICSENS.2014.6984972](https://doi.org/10.1109/ICSENS.2014.6984972).
- [8] J. Hecht, "Bringing legacy fiber optic cables up to speed," [Online]. Available: <https://spectrum.ieee.org/tech-talk/telecom/internet/legacy-fiber-optic-cables-speed-data-rates>
- [9] C. Li, T. Li, G. Guelbenzu, B. Smalbrugge, R. Stabile, and O. Raz, "Chip scale 12-Channel 10 Gb/s optical transmitter and receiver subassemblies based on wet etched silicon interposer," *J. Lightw. Technol.*, vol. 35, no. 15, pp. 3229–3236, Aug. 2017.

- [10] B. Smalbrugge, H. J. S. Dorren, O. Raz, and P. Duan, "Demonstration of wafer scale fabrication of 3-D stacked transmitter and receiver modules for optical interconnects," *J. Lightw. Technol.*, vol. 31, no. 24, pp. 4073–4079, Dec. 2013.
- [11] F. E. Doany *et al.*, "Terabit/s-class optical PCB links incorporating 360-Gb/s bidirectional 850 nm parallel optical transceivers," *J. Lightw. Technol.*, vol. 30, no. 4, pp. 560–571, Feb. 2012.
- [12] S. Fandrey, S. Weiss, and J. Müller, "A novel active MR probe using a miniaturized optical link for a 1.5-T MRI scanner," *Magn. Reson. Med.*, vol. 67, no. 1, pp. 148–155, 2012, doi: [10.1002/mrm.23002](https://doi.org/10.1002/mrm.23002).
- [13] J. Li, V. Henneken, M. Louwerse, and R. Dekker, "Optical data link module for data transmission in smart catheters," *Int. Symp. Microelectron.*, vol. 2020, no. 1, pp. 169–173, Jan. 2021, doi: [10.4071/2380-4505-2020.1.000169](https://doi.org/10.4071/2380-4505-2020.1.000169).
- [14] B. Mimoun, V. Henneken, A. Van Der Horst, and R. Dekker, "Flex-to-rigid (F2R): A generic platform for the fabrication and assembly of flexible sensors for minimally invasive instruments," *IEEE Sens. J.*, vol. 13, no. 10, pp. 3873–3882, Oct. 2013, doi: [10.1109/JSEN.2013.2252613](https://doi.org/10.1109/JSEN.2013.2252613).
- [15] M. Kluba, B. Morana, A. Savov, H. van Zeijl, G. Pandraud, and R. Dekker, "Wafer-scale integration for semi-flexible neural implant miniaturization," *Proceedings*, vol. 2, no. 13, p. 941, 2018, doi: [10.3390/proceedings2130941](https://doi.org/10.3390/proceedings2130941).
- [16] S. H. Lee, K. N. Chen, and J. J. Q. Lu, "Wafer-to-wafer alignment for three-dimensional integration: A review," *J. Microelectromech. Syst.*, vol. 20, no. 4, pp. 885–898, 2011, doi: [10.1109/JMEMS.2011.2148161](https://doi.org/10.1109/JMEMS.2011.2148161).
- [17] M. Kluba, A. Arslan, R. Stoute, J. Muganda, and R. Dekker, "Single-Step CMOS compatible fabrication of high aspect ratio microchannels embedded in silicon," *Proceedings*, vol. 1, no. 4, p. 291, 2017, doi: [10.3390/proceedings1040291](https://doi.org/10.3390/proceedings1040291).
- [18] M. van der Kaay, "High density flexible interconnect for minimally invasive medical instruments," MSc Dissertation. Dept. Microelectron., TU Delft, 2017. [Online]. Available: <https://repository.tudelft.nl/islandora/object/uuid:37e8312d-0f56-4803-8ef4-60b4f9dac5c3>